Relevance of zeta potential as a tool for predicting the response of controlled salinity waterflooding in oil-water-carbonate systems

Romain Rodrigues, Michael Levant, Alexandra Klimenko

Relevance of zeta potential as a tool for predicting the response of controlled salinity waterflooding in oil-water-carbonate systems

Romain Rodrigues[1,2,3], Michael Levant[1,2], Alexandra Klimenko[1,2*]

[1] Laboratoire Physico-Chimie des Interfaces Complexes, CHEMSTARTUP, RD 817, 64170 Lacq, France

[2] TotalEnergies, Pôle d'Etudes et Recherche de Lacq (PERL), BP 47, 64170 Lacq, France

[3] Laboratoire Sciences et Ingénierie de la Matière Molle, ESPCI Paris, CNRS, PSL University, Sorbonne Université, 75005 Paris, France

[*]Corresponding author: alexandra.klimenko@totalenergies.com

Abstract

Zeta potential has been proposed as a key parameter for predicting the response of controlled salinity waterflooding, as correlation with additional oil recovery has previously been established. However, it is unclear if there is a causal effect and if this parameter can be used as a unique predictive tool. We provide new insights with a detailed investigation into the role of the change of polarities of oil/water/rock interfaces on the additional oil recovery. Core flooding experiments with streaming potential and electrophoretic mobility measurements were performed to obtain insights into the electrostatic interactions that occur during oil recovery on Estaillades rock. Two different injection scenarios were followed in one crude oil/brine/rock (COBR) system: one conventional injection with decreasing salinity and one inverse injection with increasing salinity.

Results indicated that oil recovery in secondary mode was more important using formation brine compared to low salinity brine. Also, almost no additional oil recovery was observed in tertiary mode irrespective of the injection scenario. Rock/water zeta potential was found positive in formation brine, and negative in the low salinity brines. The determination of oil/water polarity was more difficult as

many inconsistencies between streaming potential and electrophoretic mobility measurements were observed. We propose several explanations for these discrepancies, including that the difference in zeta potential at fully water saturation and at residual saturation is not necessarily dependent on oil polarity as it can be induced by a change in rock exposed surface and in the distribution in water flow paths during measurements. The overall results suggest that zeta potential cannot be used as a unique indicator to predict the low salinity response of a COBR system.

Keywords: EOR, streaming potential, electrophoretic mobility, electrostatic interactions, rock/water interface, oil/water interface.

1. Introduction

Improving the oil recovery efficiency in carbonate reservoirs has been the subject of much research in the last decades. Indeed, while carbonate rocks contain more than 60 % of crude oil reserves [1], the average recovery factor is generally lower than 40 % [2]. This can be related to the tendency of carbonates to be more oil-wet than sandstones. Many techniques have thus been developed for enhanced oil recovery (EOR) [3,4]. It has been shown in both laboratory experiments and field trials that the total oil recovered can significantly be increased by diluting the injected brine and/or by controlling its chemical composition. This method is either called low salinity waterflooding (LSW), controlled salinity waterflooding (CSW), or smart water injection methods (SWIM) [5,6]. However, some studies on field cases have failed to observe a low-salinity effect (LSE) in several crude oil-brine-rock (COBR) systems [7].

One of the main reasons behind these inconsistencies can be related to the absence of consensus on the optimum composition of the brine to be injected. This can be explained by the fact that the mechanism of CSW is not fully understood [8–13]. It is widely accepted that additional recovery is primarily accompanied by wettability alteration to a less oil-wet state [14]. However, modification of many parameters can result in wettability alteration, and the most common suggested mechanisms

47 are mineral dissolution, surface charge alteration by multi-ionic exchange, or double layer expansion
48 [15–20]. In recent years, many studies have highlighted the importance of the oil/water interactions
49 in impacting the LSE, especially with the spontaneous formation of water-in-oil micro-droplets [21–
50 24], and thus on the importance of oil/water interface in the mechanism of additional recovery
51 [25,26]. Hence, both rock/water and oil/water interactions are important to understand LSE.

52 Considering both interfaces, Jackson et al. [27] suggested that the modification of the injected brine
53 salinity or composition must result in repulsive electrostatic forces between rock/water and oil/water
54 interface (*i.e.*, increasing the disjoining pressure) in order to observe the formation of a stable water
55 film between rock surface and oil, resulting in the detachment of oil from rock surface. Experimentally,
56 this means that the zeta potential of both interfaces must exhibit the same polarity after changing the
57 brine composition to observe additional oil recovery.

58 To determine zeta potential, many studies have shown the great interest in the measurement of
59 streaming potential in geological applications, both in saturated and unsaturated conditions [28–31].
60 Streaming potential correspond to the potential difference at zero current that develops across a
61 porous medium when charges from the diffuse layer accumulate downstream as a result of an applied
62 pressure gradient [32]. This parameter is advantageous for determining zeta potential as it can be
63 measured on intact rock samples, in high salinity conditions, and at elevated temperatures, allowing
64 the determination of zeta potential in conditions relevant to EOR [33]. It was notably shown that zeta
65 potential measured with powder samples can be very different to the one measured with intact rocks,
66 as the dominant mineral surfaces exposed to the brine in the pore structure is lost after crushing the
67 rock [34].

68 It is well established that in fully water-saturated conditions, the streaming potential is directly related
69 to zeta potential of rock/water interface [33]. This parameter is first dependent on the nature of the
70 rock. For example, among carbonates, dolomite exhibits the most positive zeta potential, while chalk
71 exhibit the most negative [16]. Zeta potential can also be modified by adjusting the nature and content

in potential determining ions present in the brines [35,36]. For example, increasing pCa or pMg results in a decrease in positive surface charges [15,37,38]. The pH and pSO_4 have only an indirect influence on zeta potential by moderating the equilibrium pCa [35,37], while other ions such as Na^+ and Cl^-, often argued as indifferent ions, may affect zeta potential due to their adsorption on calcite surface [39]. Finally, the influence of temperature is sample specific, and the dependance of zeta potential to the temperature appears correlated to the dependance of pCa to the temperature [40].

In addition to rock/water interface, the beforementioned hypothesis also required to measure oil/water zeta potential to determine the total electrostatic interactions in the system. As this measurement is often challenging in high salinity conditions using conventional electrophoretic mobility measurements, Jackson et al. proposed that the difference in zeta potential measured at fully water saturation (Sw = 1) and at residual oil saturation (Sor) after waterflooding provides a qualitative indication of the polarity of the oil/water interface due to its influence on the global zeta potential [27]. Considering that this difference is only influenced by oil properties, the authors found a correlation between additional oil recovery and the change in rock/water polarity after CSW. They notably proposed that when oil/water is identified to be positively-charged, the water composition must be changed to obtain a positive rock/water zeta potential, suggesting that it must be required to increase the salinity of the injected brines in this case [27]. However, in more recent studies, they have noted that this difference can be influenced by rock surface composition and texture [34] and brine salinity and composition [41]. Also, they observed one specific case where it was not possible to correctly predict the response, which questions a possible causal relationship between electrostatic repulsion and additional oil recovery. An absence of clear correlation has also been observed by other authors [42,43]. Hence, interpretation must be done case by case to determine the efficiency of CSW on the COBR system under consideration.

The objective of this study was to investigate if the hypothesis that the same polarity for both rock/water and oil/water interfaces, induced by a change in water composition, can predict the

response of a COBR system to CSW. The focus was thus on the calculation of rock/water and oil/water zeta potentials to determine if zeta potential can be used as a unique indicator, while the other parameters of interest, such as mineral heterogeneity or interfacial tension, were supposed to remain constant when using the same rocks and brines. It was also checked that interfacial tension changes little between brines tested. We use core flooding experiments coupled with streaming potential and electrophoretic mobility measurements following two different injection scenarios: one conventional injection with decreasing salinity from formation brine to low salinity brine, and one inverse injection with increasing salinity from low salinity brine to formation brine. The results are then interpreted according to the hypothesis to determine both interfaces' polarity and conclude concerning its predictive capacity. Finally, a more general discussion with results from other publications in a similar COBR system is proposed.

2. Materials and methods

2.1. Rock and fluid properties

Experiments were performed using Estaillades (EST) limestone samples (> 98% of calcite), quarried in France, which exhibit a bimodal pore throat distribution [44], as shown in Figure S1. Cylindrical samples of 30 cm in length and 3.9 cm in diameter were used. The main properties of the rock samples are described in Table 1.

Three brines, namely formation brine (FMB), desulfated sea water (SW-SO4), and 40-times diluted sea water (SWd40), were prepared by dissolving salts (≥ 98.5 % grade) in deionized water (ρ > 10 MΩ cm). The composition of the prepared solutions is presented in Table 1 and is globally comparable to the brines used in other studies [34,41,45,46]. Here, the objective was not to optimize the composition in term of ionic composition and concentration to improve the recovery factor, but to induce a change in zeta potential polarity and to compare two different injection scenarios with model solutions. Hence, desulfated sea water was mainly used because of constraints in field application rather than to modify zeta potential values.

122 **Table 1.** Description of the materials used in this study.

Rock properties

Parameters	Sample EST1 (conventional flooding)	Sample EST2 (inverse flooding)
Gaz permeability (mD)	258	220
Pore volume PV (mL)	114	116.5
Porosity (%)	32.2	32.7
Longitudinal dispersivity coefficient α (cm)	0.4-0.5	0.45-0.55

Brine compositions and properties

Salt (before pre-equilibration)	SWd40 (g L^{-1})	SW-SO4 (g L^{-1})	FMB (g L^{-1})
NaCl (VWR, AnalaR Normapur)	0.76	29	109.55
KCl (Fisher, ≥ 99%)	0.035	0.9	0
$CaCl_2$, $2H_2O$ (Merck, ≥ 99%)	0.020	0.605	46.07
$MgCl_2$, 6 H_2O (Fisher, ≥ 99%)	0.296	0.405	11.24
Na_2SO_4 (VWR, AnalaR Normapur)	0.087	0.026	0.14
$NaHCO_3$ (Merck, ≥ 99%)	0.0007	0.156	0.20
Ionic strength (mol L^{-1})	0.02	0.53	2.99
Conductivity (S m^{-1})	0.42 (EST1)	9.0 (EST1)	31.1 (EST1)
(70 °C, after pre-equilibration)	0.49 (EST2)	8.9 (EST2)	30.2 (EST2)

Oil properties

Density at 70 °C (g cm^{-3})	0.81
Viscosity at 70 °C (mPa s)	1.52
Total acid number (mg KOH g^{-1})	0.34
Total base number (mg KOH g^{-1})	0.41
Saturates (wt%)	48.4
Aromatics (wt%)	48.1
Resins (wt%)	2.8
Asphaltenes (wt%)	0.7

123

124 After preparation, rock pieces were introduced in each solution for pre-equilibration for at least 2
125 weeks to limit further core dissolution and to shorten the equilibration time with the intact rocks
126 during core flooding. Before use, the brines were filtered with a vacuum pump through a 0.45 µm
127 filter. The impact of filtration was supposed to be small as the variation in conductivity before and
128 after filtration was lower than 1 %.

The crude oil, named Oil T, was used with its main characteristics presented in Table 1. Mineral oil Marcol 82 (ExxonMobil, μ = 5.4 mPa s at 70 °C) was used for drainage to reach the targeted water saturation.

2.2. Experimental procedure

A schematic representation of the experimental setup is shown in Figure 1. It is an adaptation of the experimental procedure developed by Jackson et al. [27] and used by Levant et al. [32], the main difference being the size of the rock sample and the drainage protocol. The carbonate sample was fitted in a Viton rubber sleeve and inserted into a vertical Hassler-type core holder in which mineral oil (Marcol 82) was used to apply a confining pressure of 40 bars. Once the pressure has stabilized, the pore volume (PV) and permeability were determined by gas. The rock sample was then swept with CO_2 and vacuumed several times before vacuum saturation with SWd40 (Sw = 1). The PV and the longitudinal dispersivity coefficient were then measured using a tracer test with potassium iodide (KI) by following the evolution of absorbance in UV using an UPC-900 monitor. The cell was finally placed in an oven at T = 70 °C.

All elements in the setup, *i.e.* tubings and valves, were made in PFA or PEEK. Hence, no metallic elements were in contact with the brines to eliminate any current that could affect the value of streaming potential (j = 0). Measurements were first carried out at Sw = 1 in a closed system. The brine of interest was placed inside two homemade PVC cylinders and the flow was initiated by the injection of Marcol 82 in the cylinders using an ISCO pump. The direction of the flow can be reversed during measurement – from bottom to top or top to bottom – to verify the symmetry of the signal. Measurements at Sw = 1 were performed in the order SWd40 → SW-SO4 → FMB. At least 3 PVs were injected for the replacement of each brine, and each measurement was done after an equilibration time of at least 24 h with the intact rock at elevated temperature.

Drainage of FMB-filled core was achieved by injecting Marcol 82 from top to bottom until reaching an irreducible water saturation (Swi) of about 27-28%. During the increase in flowrate, the confining

pressure was increased to maintain it at least 20 bars higher than the pore pressure. The total volume of water recovered during this step was used to determine the oil in place (OIP). Then, approximately 2.5 PVs of toluene were injected at a low flowrate (approximately 0.05 PV h^{-1}) to avoid mixing of mineral oil with crude oil and to prevent possible precipitation of asphaltenes from the crude oil. Oil T is finally filtered in line (0.5 µm) and injected at a low flowrate into the medium. At least 5 PVs were injected to ensure the proper replacement of toluene, which was verified by measuring oil density and viscosity at the outlet with a SVM 3000 viscometer (Anton Paar).

Afterwards, an ageing step of the core was performed to obtain a rock wettability more representative of reservoir conditions. This step was carried out by isolating the core at 90 °C for 2 weeks, with the replacement of one PV of oil at a low flowrate after the first week. Oil permeability was measured before and after ageing, but no significant difference was observed for both experiments.

Core waterflooding in gravity stable manner (from bottom to top) was then initiated at 70 °C using either a conventional flood by decreasing the salinity for EST1 (FMB → SW-SO4 → SWd40) or an inverse flood by increasing the salinity for EST2 (SWd40 → SW-SO4 → FMB). The initial flowrate was ≈ 4.5-5 mL h^{-1}, which correspond to an interstitial velocity of about 1 ft day^{-1}. The volume of oil recovered into a graduated burette was automatically monitored. When this volume no longer varied, the flowrate was gradually increased, up to 6.5 PV h^{-1}, to obtain a pressure drop of about 2 bars to reduce capillary end effect, to approach the residual oil saturation (Sor) value, and to obtain a better signal-to-noise ratio for streaming potential measurements at high salinity. When only water is produced at the final flowrate, the streaming potential was measured at Sor with the same methodology as described before. The same procedure was applied after switching to the next brine of interest to measure any additional oil recovery and streaming potential.

At the end of the experiments, the mass balance was verified by extracting the water of the rock in a Dean-Stark apparatus using toluene as solvent. In both cases, the difference between oil saturation defined by mass balance by distillation was about 5-10 %.

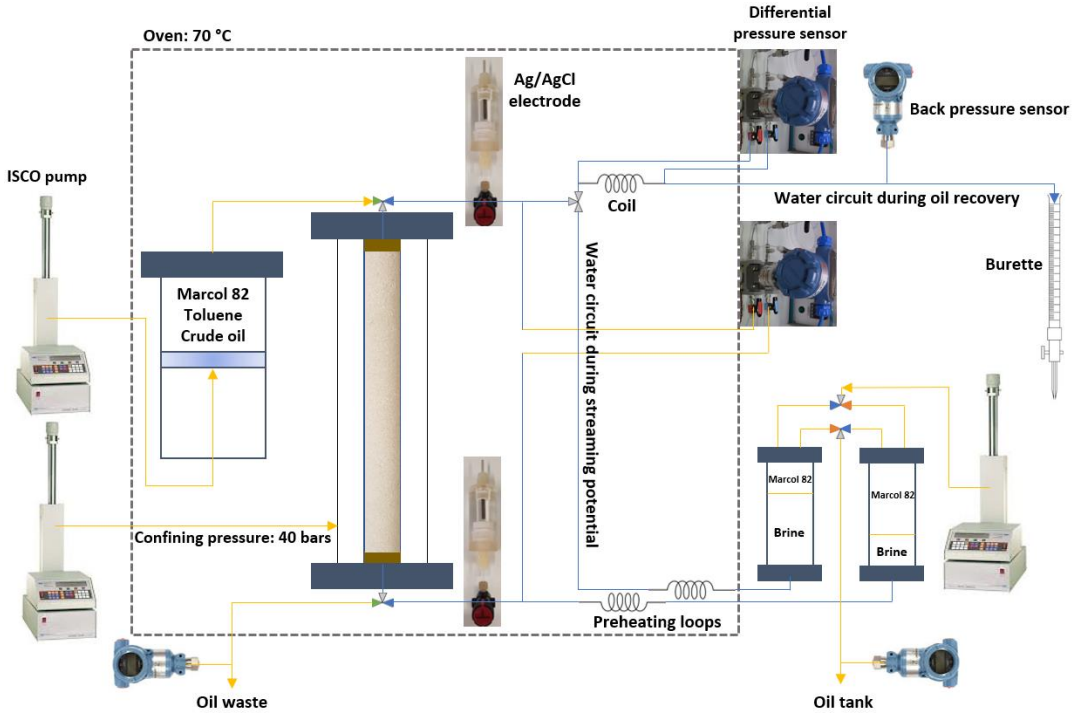

Figure 1. Schematic representation of the experimental setup for core flooding experiments with streaming potential measurements.

2.3. Calculation of zeta potential from streaming potential measurements

Zeta potential was calculated using Helmholtz-Smoluchowski equation (Eq. 1) based on a bundle of capillary tubes model, already used by Jackson et al. [27] for carbonates:

$$\zeta = \frac{C\mu_w\sigma_{rw}F}{\varepsilon_w} \approx \frac{C\mu_w\sigma_w}{\varepsilon_w} \quad \text{(Eq. 1)}$$

with C the electrokinetic coupling coefficient, which relates the streaming potential (ΔE) and pressure gradients (ΔP) when the total current density is null ($C = \Delta E/\Delta P$, V Pa^{-1} for j = 0 A), μ_w the water dynamic viscosity (Pa s), σ_w the water conductivity (S m^{-1}), and ε_w the water dielectric constant (F m^{-1}). The pore size of Estaillades is globally sufficiently large to justify the use of the Helmholtz-Smoluchowski relationship [47]. The use of the relationship with the surface conductivity σ_{rw} and the formation factor F was not required because the contribution of the surface conductivity can be neglected due to the concentrations of the solutions used (I > 0.01 M) [48]. Surface conductivity was only measured in previous experiments using internal Ag/AgCl electrodes [32] (see Figure S2) and formation factor values were comprised between 14 and 18 for the three brines at Sw = 1.

While applying a flowrate, the pressure difference across the porous medium Δ*P* was measured using a differential sensor (Rosemount 3051), calibrated between -5 and +5 bars using a HART field communicator. The resulting streaming potential Δ*E* across the porous media was measured using a pair of non-polarizable Ag/AgCl electrodes. There were prepared by electrodeposition of AgCl on silver rods (65×3 mm, Advent), applying a DC current of ≈50 µA during 30 s in a 2 M NaCl solution. Each electrode was then inserted into a homemade PMMA housing with two compartments (see Figure 1) separated by a sintered glass membrane (Verres Vagner) [32], used to isolate each Ag/AgCl electrode from the flow line to obtain a better electrical stability. Both compartments were filled with the brine of interest, ensuring the absence of any bubbles.

The pressure sensor and the electrodes were then connected to a NI-9219 acquisition system, using the ± 125 mV voltage range with high impedance (> 1 GΩ), for data acquisition and recording via a modified version of a home-made software previously developed on LabVIEW [32]. The use of a high-impedance system was required to accurately determine the coupling coefficient as the resistance of the system was high using SWd40, as shown in Figure S3. Figure 2 shows typical results obtained for the measurements of Δ*E* and Δ*P*, at several increasing flowrates, in both flow directions (bottom to top and top to bottom, represented as positive and negative pressures respectively). The determination of coupling coefficients *C* in SWd40, SW-SO4, and FMB using the paired stabilization method, i.e. after reaching the most stable values for Δ*E* and Δ*P*.

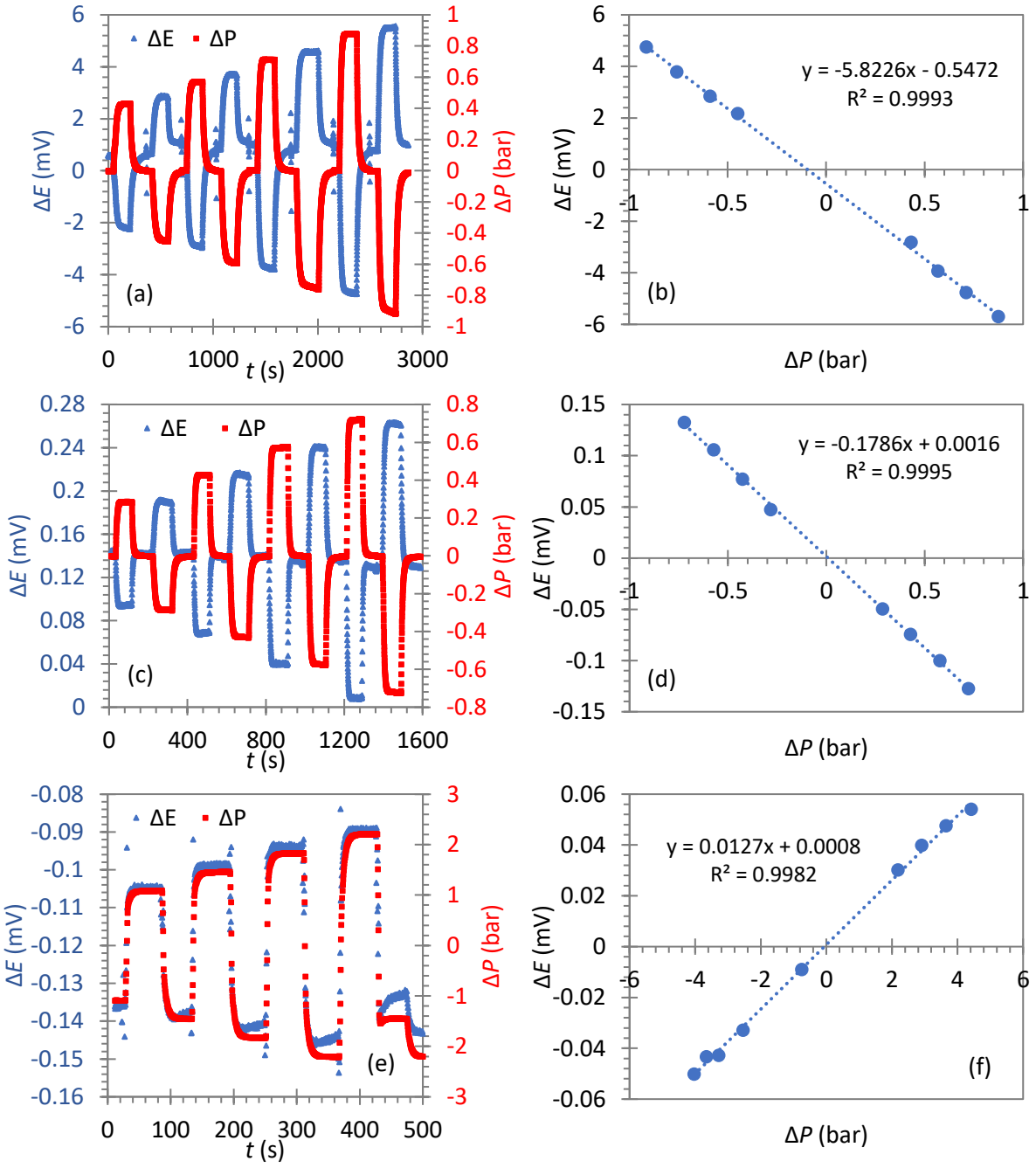

Figure 2. Example of measurements of streaming potential Δ*E* and pressure gradient Δ*P* vs time and determination of electrokinetic coupling coefficients *C* in (a and b) SWd40, (c and d) SW-SO4, and (e and f) FMB brines. The raw data (left) represent the variation of Δ*E* and Δ*P* while applying different flowrates in each direction (positive and negative pressure) until reaching the most stable values. As the magnitude of variations in Δ*E* in FMB is very small (a few tens of µV for high Δ*P*), a good equilibration and data acquisition system with very high resolution are required.

The brines in the two PVC cylinders used for streaming potential measurements were then collected, and the pH and conductivity were measured at 70 °C using a combined glass electrode (ThermoScientific Orion 8157BNUMD), calibrated with pH buffer 7 and 10, and a four-pole electrode (ThermoScientific Orion 013005MD), respectively, connected to Orion VersaStar Pro multimeter

(Thermo Scientific). Water viscosity μ_w was determined by measuring the pressure difference ΔP of a metallic capillary previously calibrated at 70 °C using demineralized water with known viscosity. The water viscosity was then calculated with Poiseuille's law (Eq. 2):

$$\mu_w = \frac{\Delta P \pi r^4}{8LQ} \quad \text{(Eq. 2)}$$

with r the diameter of the capillary (m), L the length of the capillary (m), and Q the flow rate ($m^3\ s^{-1}$).

From the viscosity, the water permeability of the core sample was then calculated using Darcy's law (Eq. 3):

$$k = \frac{Q \mu_w L}{A \Delta P} \quad \text{(Eq. 3)}$$

with k the permeability (m^2), L the length of the core sample (m), A the flow cross section (m^2) and ΔP the total pressure difference across the porous medium (Pa).

The dielectric permittivity of bulk water ε_w was calculated by first determining the relative permittivity ε_f according to the following empirical relation (Eq. 4) [28]:

$$\varepsilon_f = 295.68 - 1.2283\,T + 2.094\,10^{-3}\,T^2 - 1.41\,10^{-6}\,T^3 \quad \text{(Eq. 4)}$$

The influence of salt such as NaCl was considered using the relation (Eq. 5) [28]:

$$\varepsilon_f = \varepsilon_f(T) - 13\,C_f + 1.065\,C_f^2 + 0.03006\,C_f^3 \quad \text{(Eq. 5)}$$

with C_f the salt concentration (mol L^{-1}). The dielectric permittivity is finally calculated by (Eq. 6):

$$\varepsilon_w = \varepsilon_f \varepsilon_0 \quad \text{(Eq. 6)}$$

with ε_0 the vacuum permittivity ($8.854\ 10^{-12}$ F m^{-1}). One should note that the dielectric permittivity is calculated according to the theoretical composition of the bulk solutions with Eqs. 4-5, without considering the hydrophilicity/hydrophobicity of the surface. Also, it was considered uniform and

constant despite being space-dependent [49]. With these assumptions, they can be used for a comparative purpose when the same brine is used.

The uncertainty in zeta potential value $u(\zeta)$ was determined according to the relationship (Eq. 7):

$$u(\zeta) = \left(\frac{u(C)}{|C|} + \frac{u(\mu_w)}{\mu_w} + \frac{u(\sigma_w)}{\sigma_w}\right) * |\zeta| \quad \text{(Eq. 7)}$$

The uncertainty in the value of the coupling coefficient *C* corresponds to the 95% uncertainty obtained from the linear regression of the experimental data. The uncertainty in conductivity (and pH) values corresponds to the standard deviation based on three measurements. The uncertainty is slightly underestimated because it does not consider the uncertainty of the dielectric permittivity.

2.4. Determination of oil/water polarity by streaming potential measurements (SPM)

We use the hypothesis that the difference in zeta potential values obtained by streaming potential measurements between the core in fully water-saturated conditions (Sw = 1) and the core at residual oil saturation (Sor) can provide qualitative insights into the polarity of the oil/water interface [27,41]. The difference between the two measurements is calculated according to the formula (Eq. 8):

$$\Delta\zeta = \zeta_{\mathrm{Sor}} - \zeta_{\mathrm{Sw=1}} \quad \text{(Eq. 8)}$$

As previously mentioned, measurements performed at Sw = 1 are indicative of the sign and magnitude of zeta potential of the rock/water interface. At Sor, the zeta potential value is expected to be modified only by the presence of residual oil. Indeed, it was shown that, as long as the fluid resistivity remains small (*i.e.*, high ionic concentration), the electrokinetic coupling coefficient is almost not impacted by the pore size distribution and the permeability [50–52], which are expected to change between the two conditions.

An illustration of the different possibilities proposed by Collini et al. [41] is presented in Figure 3.

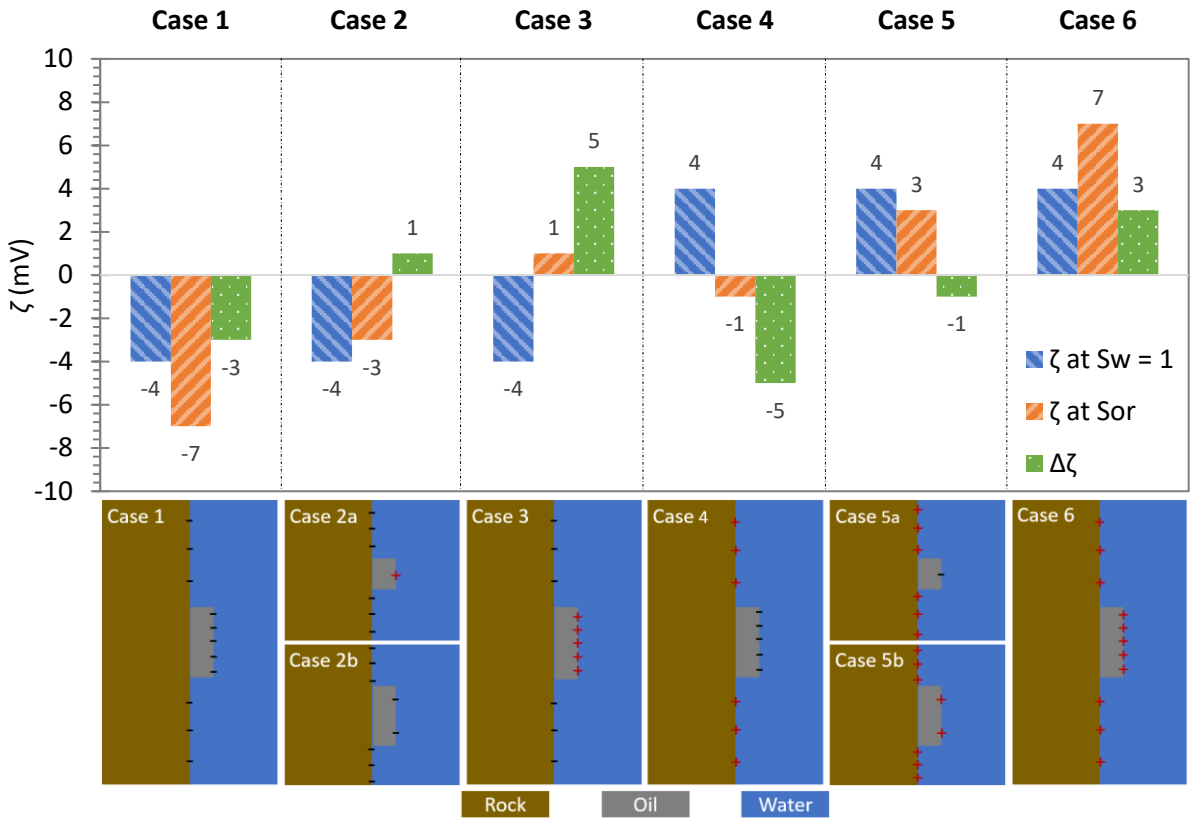

Figure 3. Illustration of the different possibilities for the difference of zeta potential between Sw = 1 and Sor, according to [41]. According to the tested hypothesis, the oil/water polarity can be determined without ambiguity for Case 1 (ζ is significantly more negative at Sor than at Sw = 1), Case 3 (ζ is negative at Sw = 1 and becomes positive at Sor), Case 4 (ζ is positive at Sw = 1 and becomes negative at Sor) and Case 6 (ζ is significantly more positive at Sor than at Sw = 1). For Case 2, in which ζ is less negative at Sor, ζ of oil/water can either be positive (Case 2a) or less negative (Case 2b) than rock/water interface. In the same way, for Case 5, in which ζ is less positive at Sor, ζ of oil/water can either be negative (Case 5a) or less positive (Case 5b) than rock/water interface. The different cases are also represented with a simplified illustration of the COBR system, in which (i) the rock surface is represented as flat, (ii) the surface charge is homogeneously distributed on the rock surface, and (iii) there is no preferential sites for oil adsorption on the rock surface.

The different scenarios are:

- Case 1: if zeta potential is more negative at Sor than at Sw = 1, the oil/water interface should be negative.
- Case 2: if zeta potential is less negative at Sor than at Sw = 1, the oil/water interface should either be positive (2a) or less negative (2b) than the rock/water interface, depending on rock cover fraction.
- Case 3: if zeta potential is negative at Sw = 1 and becomes positive at Sor, the oil/water interface should be positive.

- Case 4: if zeta potential is positive at Sw = 1 and becomes negative at Sor, the oil/water interface should be negative.
- Case 5: if zeta potential is less positive at Sor than at Sw = 1, the oil/water interface should either be negative (5a) or less positive (5b) than the rock/water interface, depending on rock cover fraction.
- Case 6: if zeta potential is more positive at Sor than at Sw = 1, the oil/water interface should be positive.

Whatever the case, it seems possible to express ζ at Sor, with some simplifications, as (Eq. 9):

$$\zeta \text{ at Sor} = \zeta_{\mathrm{r/w}} * \frac{A_{\mathrm{r/w}}}{(A_{\mathrm{r/w}} + A_{\mathrm{o/w}})} + \zeta_{\mathrm{o/w}} * \frac{A_{\mathrm{o/w}}}{(A_{\mathrm{r/w}} + A_{\mathrm{o/w}})} \quad \text{(Eq. 9)}$$

with $A_{r/w}$ the rock surface exposed to water and $A_{o/w}$ the oil surface exposed to water (with $A_{r/w} + A_{o/w}$ = 100 %). It is easy to show that:

- $\zeta_{o/w} > 0$ if $\zeta \text{ at Sor} > \zeta_{r/w} * (1 - \frac{A_{o/w}}{(A_{r/w}+A_{o/w})})$;
- $\zeta_{o/w} < 0$ if $\zeta \text{ at Sor} < \zeta_{r/w} * \left(1 - \frac{A_{\frac{o}{w}}}{(A_{r/w}+A_{o/w})}\right)$.

For Cases 2 and 5, the same value of ζ at Sor can be obtained with different polarity of oil/water interface, depending on the rock surface covered by the remaining oil. For example, considering the hypothetic Case 2 where $\zeta_{r/w}$ = - 4 mV, to obtain ζ at Sor = - 3 mV, $\zeta_{o/w}$ = + 1 mV for $A_{o/w}$ = 20 % but $\zeta_{o/w}$ = - 2 mV for $A_{o/w}$ = 50 %. Finally, the absence of significant difference between the values at Sw = 1 and at Sor can indicate that zeta potentials of rock/water and oil/water interfaces are in the same order of magnitude.

2.5. Determination of oil/water zeta potential by electrophoretic mobility measurements (EPM)

Measurements of oil/water zeta potentials were carried out using a Zetasizer Nano-ZS (Malvern Instruments), which measures the electrophoretic mobility u_e (µm cm V^{-1} s^{-1}) of droplets in suspension. Zeta potential is then determined using Smoluchowski approximation of Henry's equation (Eq. 10) [53]:

$$\zeta = \frac{u_e \mu_w}{\varepsilon_w} \quad \text{(Eq. 10)}$$

The solution was prepared by first manually mixing 2 mL of oil T in a total volume of 20 mL using the brine of interest (volume ratio of 1:10). Then, a small volume of the suspension was gently introduced in a disposable capillary cell (DTS1070, Malvern Instruments). The cuvette was thermalized within the instruments at 70 °C and measurements were done for the three brines of interest to obtain insights on the sign and the order of magnitude of the oil/brine zeta potential. Five measurements with five runs each were performed to determine the average zeta potential with its standard deviation.

It is important to note that this method may not be very reliable at high salinities because of its intrinsic limitations. Indeed, the low electrophoretic mobility in a highly conductive solution can require very high voltage across the cell, which causes significant Joule heating and affects the accuracy and quality of the measurements [54].

3. Results

3.1. Oil recovery

Results of oil recovery of both core floodings are presented in Figure 4.

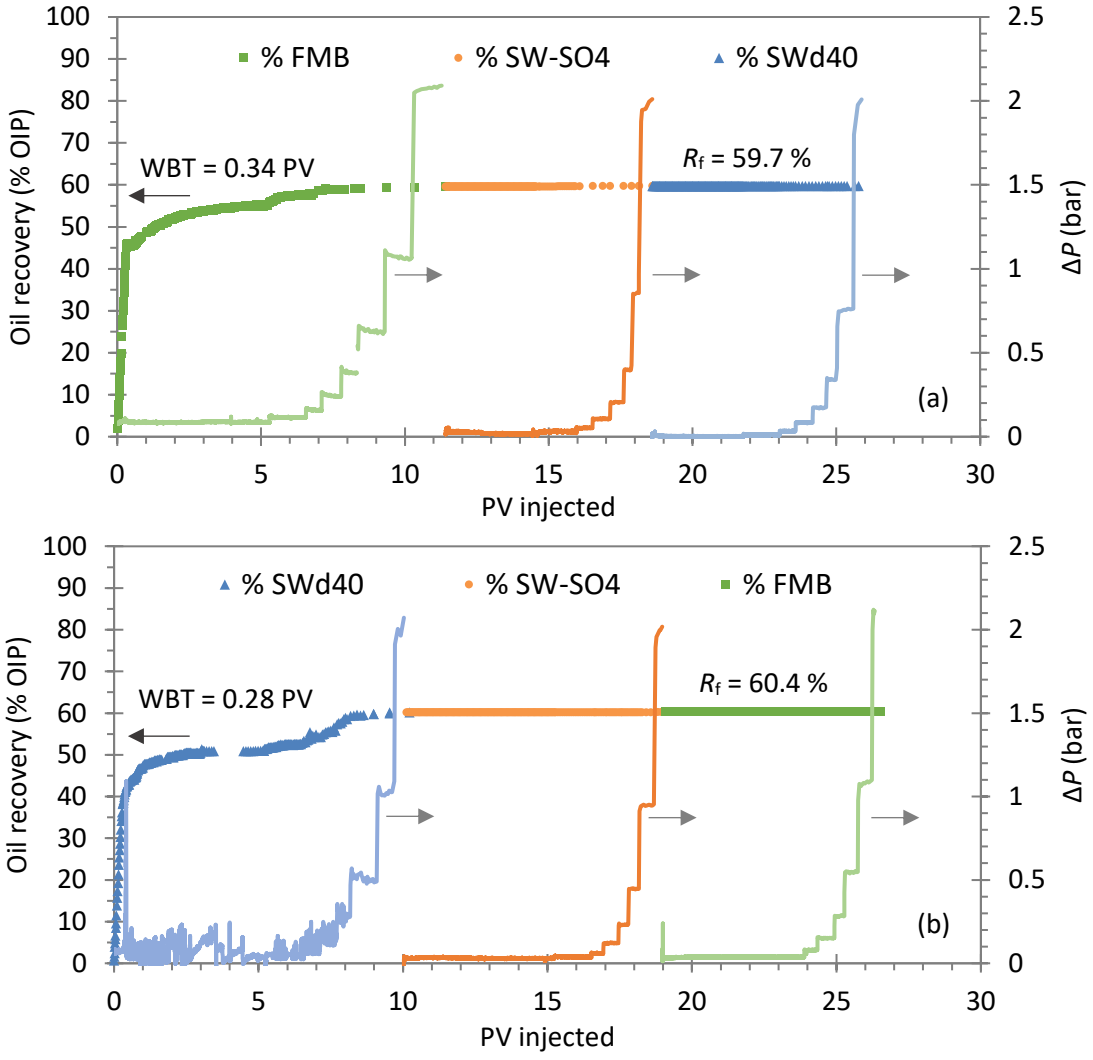

Figure 4. Kinetics of oil recovery expressed as %OIP and evolution of Δ*P* during core flooding at 70 °C with (a) decreasing salinity from FMB to SWd40 (EST1) and (b) increasing salinity from SWd40 to FMB (EST2). Δ*P* was noisy during the injection of SWd40 in secondary mode due to the instability of the back-pressure regulator.

When FMB is injected in secondary mode (Figure 4a), the water breakthrough (WBT) is observed at 0.34 PV, and it takes more than 4.5 PVs to observe the plateau of oil production at the first flowrate, which corresponds to a recovery of 55.1 %. The increase in flowrate results in the production of additional oil with a final recovery of 59.5 % after the last bump rate, which evidences the presence of capillary end effect and indicates not strongly water-wet wettability state.

When SWd40 is injected in secondary mode (Figure 4b), the WBT is observed more rapidly, at 0.28 PV, and the oil production plateau is already observed after 3.5 PVs, much more rapidly than using FMB. At the end of the injection at the first flowrate, the recovery is 51 %, *i.e.* 4.1 % less than with FMB. As only one experiment was performed for each injection sequence, it is not possible to state that this

difference is significant. With the increase in flowrate, the total oil recovered reached 60.1 %, which indicates again the presence of capillary end effect and not strongly water-wet porous media.

Irrespective of the order of injection of the brines (decreasing or increasing salinity), almost no additional oil recovery was observed after switching the brine in tertiary mode. The final recovery reached 59.7 % (+ 0.2 %) in the first case and 60.4 % (+ 0.3 %) in the second case, which corresponds to remaining oil saturation (ROS) of about 28.7 % and 28.3 %, respectively (

Table ***2***).

Table ***2*** also lists the values of water permeability for the three brines. For each experiment, permeability is globally similar between the three brines. Also, in both cases, the permeability is reduced by 30-45 % at Sor, which is related to the restriction of the water flow path because of the presence of the remaining oil.

Table 2. Variation of water permeability *k* for the three brines at 70 °C and remaining oil saturation ROS.

Experiment	**Parameters**	**FMB**	**SW-SO4**	**SWd40**
Conventional flooding (EST1)	*k* at Sw = 1 (mD)	190	192	179
	k at Sor (mD)	116	112	119
	k_{rw} at Sor	0.61	0.58	0.66
	ROS (%)	28.9	28.7	28.7
Experiment	**Parameters**	**SWd40**	**SW-SO4**	**FMB**
Inverse flooding (EST2)	*k* at Sw = 1 (mD)	167	197	186
	k at Sor (mD)	117	113	108
	k_{rw} at Sor	0.70	0.57	0.58
	ROS (%)	28.8	28.6	28.3

The relative permeability (k_r) and capillary pressure (*P*c) curves obtained by history matching with CYDAR software are shown in Figure 5, and the Corey parameters for relative permeability curves are given in Table 3. There is no major difference in terms of k_r and k_{rw}/k_{ro} curves using either FMB or SWd40 in secondary mode. Looking at Corey parameters and high values of $k_{rw,max}$, the wettability seems to be intermediate-wet in both cases. However, *P*c curves indicate that the rock seems to be slightly more oil wet for FMB than for SWd40, but it stays within the limits of error.

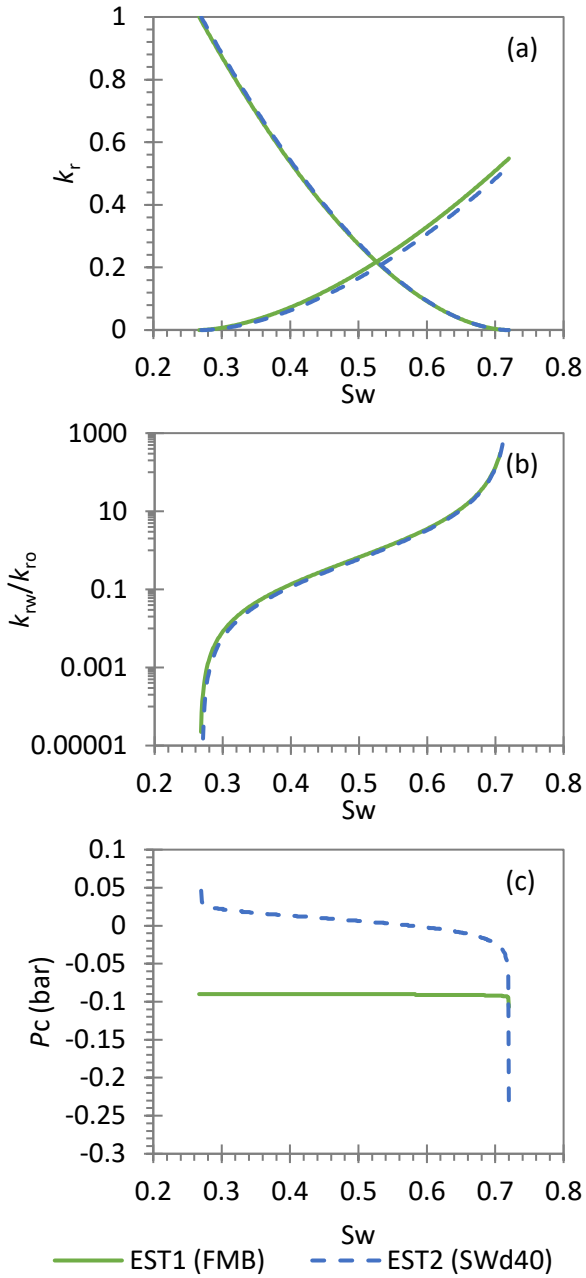

Figure 5. (a) Normalized relative permeability k_r, (b) k_{rw}/k_{ro} and (c) capillary pressure (Pc) curves obtained by history matching.

Table 3. Corey parameters for relative permeability curves.

Parameters	EST1	EST2
Swi (%)	26.7	27
Sor (%)	28	28
$k_{rw,max}$	0.55	0.52
n_w	1.653	1.711
n_o	1.792	1.791

3.2. Zeta potential

Results of zeta potentials calculated from streaming potentials at Sw = 1 and Sor are presented in Figure 6. In both experiments, values obtained at Sw = 1 (in blue on Figure 6) are negative for SWd40 and SW-SO4 and positive for FMB. As the results obtained in this condition are indicative of the rock/water interface, this interface is negative with SWd40 and SW-SO4 and positive with FMB, as already seen in previous studies using Estaillades rocks [27,34,35]. Zeta potential is more negative when decreasing brine salinity, even if the difference between SWd40 and SW-SO4 is small and appears negligeable for EST2. Overall, the evolution of zeta potential with salinity agrees with surface charge alteration by multi-ionic exchange (for the change in magnitude and sign) or double layer expansion (for the change in magnitude only).

Globally, zeta potentials obtained for EST2 are less negative for SWd40 and SW-SO4 and more positive for FMB than those obtained for EST1. This variation can be related to differences in rock texture or the presence of impurities [49,55,56], as the calculated zeta potential represents a macroscopic weighted average that accounts for the magnitude and distribution of microscopic zeta potentials arising at each mineral surfaces (Figure 7). It can also be related to the difference in the composition of the solutions after interaction with the intact sample, as some variations in pH, conductivity and viscosity were observed (

379 Table ***4***). These variations could indicate additional dissolution/precipitation occurring during the
380 contact with the intact rock, despite the pre-equilibration with rock pieces.

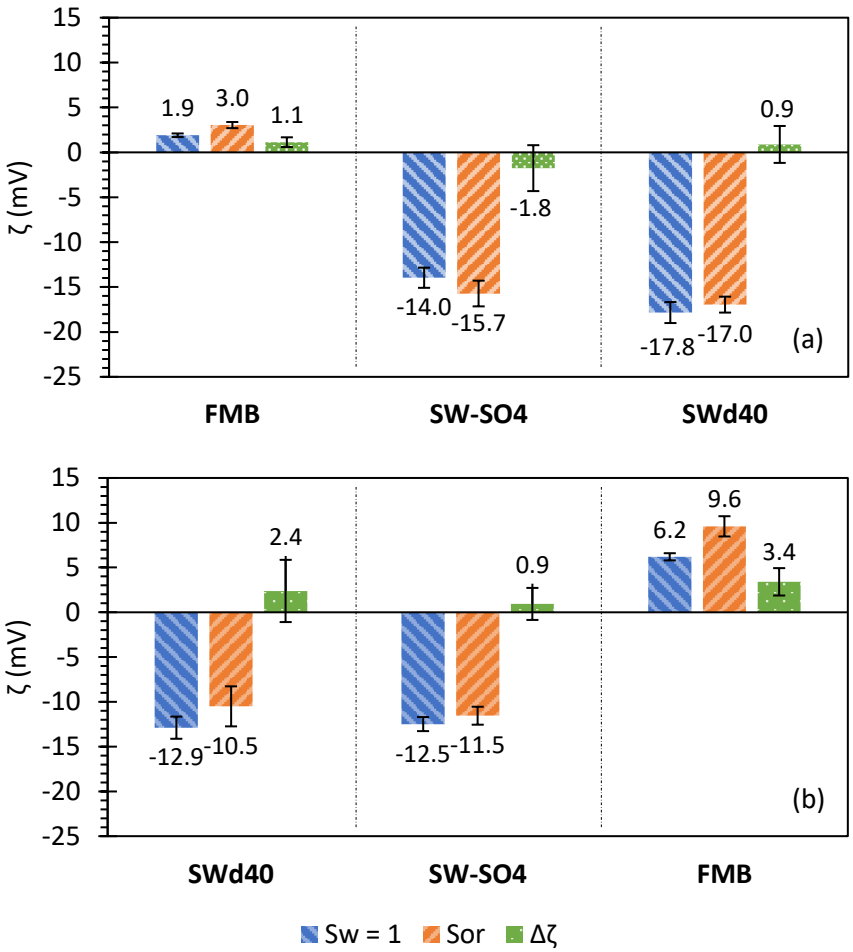

Figure 6. Comparison of zeta potential values obtained by streaming potential measurements (SPM) for SWd40, SW-SO4, and FMB between Sw = 1 and Sor obtained for core flooding at 70 °C with (a) decreasing salinity (EST1) and (b) increasing salinity (EST2). The error bars on Δζ are determined according to the maximum difference in the values obtained at Sw = 1 and Sor.

Table 4. Values of pH and the different parameters required for the calculation of zeta potential in the three brines for the two experiments measured in the equilibrated brines at 70 °C. Viscosities were not measured at Sor and were considered equal to the viscosities measured at Sw = 1.

Experiment	Water saturation	Parameters	SWd40	SW-SO4	FMB
Conventional flooding (EST1)	Sw = 1	pH	8.0 ± 0.1	8.0 ± 0.1	6.6 ± 0.1
		C (V Pa^{-1})	-5.82 10^{-8} ± 1.6 10^{-9}	-2.15 10^{-9} ± 7.6 10^{-11}	3.94 10^{-11} ± 3.2 10^{-12}
		σ_w (S m^{-1})	0.478 ± 0.005	8.70 ± 0.16	30.6 ± 0.1
		μ_w (mPa s)	0.36 ± 0.01	0.38 ± 0.01	0.47 ± 0.01
		ε_w (F m^{-1})	5.62 10^{-10}	5.07 10^{-10}	2.98 10^{-10}
		ζ (mV)	-17.8 ± 1.2	-14.0 ± 1.1	1.9 ± 0.2
	Sor	pH	7.8 ± 0.1	7.6 ± 0.1	6.7 ± 0.1
		C (V Pa^{-1})	-4.81 10^{-8} ± 1.0 10^{-9}	-2.31 10^{-9} ± 1.4 10^{-10}	6.23 10^{-11} ± 5.5 10^{-12}
		σ_w (S m^{-1})	0.550 ± 0.002	9.12 ± 0.02	30.9 ± 0.1
		μ_w (mPa s)	0.36 ± 0.01	0.38 ± 0.01	0.47 ± 0.01
		ε_w (F m^{-1})	5.62 10^{-10}	5.07 10^{-10}	2.98 10^{-10}
		ζ (mV)	-17.0 ± 0.9	-15.7 ± 1.4	3.0 ± 0.3
Inverse flooding (EST2)	Sw = 1	pH	7.6 ± 0.1	7.8 ± 0.1	6.6 ± 0.1
		C (V Pa^{-1})	-2.11 10^{-8} ± 1.0 10^{-9}	-1.79 10^{-9} ± 3.8 10^{-11}	1.27 10^{-10} ± 4.8 10^{-12}
		σ_w (S m^{-1})	0.82 ± 0.02	8.80 ± 0.15	30.0 ± 0.2
		μ_w (mPa s)	0.42 ± 0.01	0.40 ± 0.01	0.49 ± 0.01
		ε_w (F m^{-1})	5.62 10^{-10}	5.07 10^{-10}	2.98 10^{-10}
		ζ (mV)	-12.9 ± 1.2	-12.5 ± 0.8	6.20 ± 0.4
	Sor	pH	7.4 ± 0.1	7.5 ± 0.1	6.7 ± 0.1
		C (V Pa^{-1})	-1.90 10^{-8} ± 3.1 10^{-9}	-1.59 10^{-9} ± 7.2 10^{-11}	2.00 10^{-10} ± 1.8 10^{-11}
		σ_w (S m^{-1})	0.74 ± 0.02	9.20 ± 0.15	29.5 ± 0.2
		μ_w (mPa s)	0.42 ± 0.01	0.40 ± 0.01	0.49 ± 0.01
		ε_w (F m^{-1})	5.62 10^{-10}	5.07 10^{-10}	2.98 10^{-10}
		ζ (mV)	-10.5 ± 2.2	-11.6 ± 1.0	9.6 ± 1.1

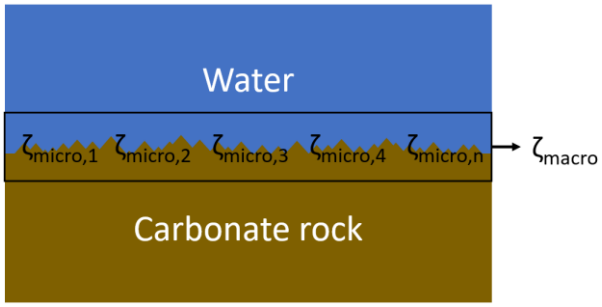

Figure 7. Schematic representation of rock/water interface with the distribution of microscopic zeta potential ζ_{micro} and the resulting macroscopic zeta potential ζ_{macro} that can be obtained with streaming potential measurements. Surface roughness can affect the measurement due to its influence on the position of the shear (or slipping) plane.

Values obtained at Sor are also negative for SWd40 and SW-SO4 and positive for FMB (orange in Figure 6). Compared to the results at Sw = 1, zeta potential is consistently more positive for FMB for EST1 and EST2, which indicates a positive oil/water interface. However, for SWd40 and SW-SO4, it is difficult to provide a definitive conclusion for each experiment as the variation falls within the experimental uncertainties. If we still consider the absolute values, zeta potentials for SWd40 are less negative at Sor in both experiments, which indicates that the oil/water interface is either less negative than the rock/water interface or positive. For SW-SO4, zeta potential at Sor is more negative for EST1 and less negative for EST2, which indicates contradictory conclusions: oil/water interface appears more negative than rock/water interface for EST1 and appears less negative than rock/water interface or slightly positive for EST2.

Some differences in pH and conductivity between Sw = 1 and Sor have been observed (

Table ***4***). These differences can be the result of further dissolution/precipitation phenomena during oil recovery but also indicates the transfer of endogenous oil species during oil-water contact [57]. As a result, the brines are not strictly identical at Sw = 1 and at Sor, which can compromise the direct comparison of zeta potentials.

Since streaming potential measurements failed to clearly define the polarity of the oil/water interface in SWd40 and SW-SO4 brines, the oil/water zeta potential was obtained by measurement of electrophoretic mobility at 70 °C. The results are presented in Figure 8. In all cases, the average values of oil/water zeta potential are negative, and the values are more negative when decreasing salinity. For FMB, it was not possible to determine without ambiguity the sign of zeta potential because of the limits of electrophoretic measurement in high saline conditions, but most measurements have resulted in negative values. It is important to note that the quality of the measurement was only satisfactory for SWd40, so the reliability of the values obtained for SW-SO4 and, especially, for FMB remains questionable.

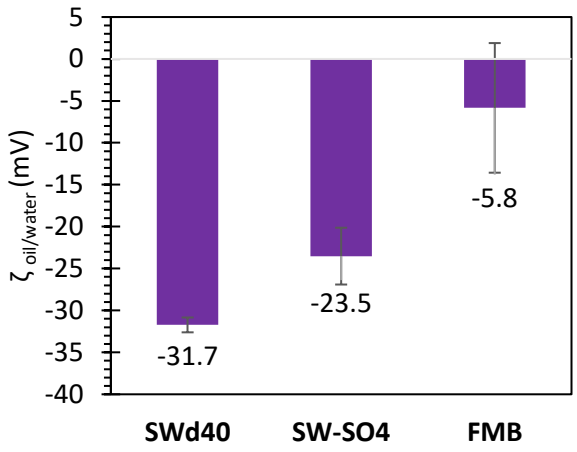

Figure 8. Zeta potential values of oil/water interface at 70 °C calculated by electrophoretic mobility measurements (EPM) with the three brines used for EST2.

4. Discussion

4.1. Application and limits of zeta potential measurements

The polarity of rock/water and oil/water interface is summarized in

Table ***5***, with their expected impact on oil recovery.

Table 5. Summary of rock/water and oil/water polarities according to streaming potential measurements (SPM) at Sw = 1 and Sor at 70 °C (according to Figure 6) or electrophoretic mobility measurements (EPM) for oil/water interface (according to Figure 8), with the predicted impact on oil recovery based on the investigated hypothesis. The presence of an asterisk denotes uncertainties on the determination of the polarity of oil/water interface. N/D: not determinable.

Experiment	Brine	Rock/water interface	Oil/water interface	Oil recovery
Conventional flooding (EST1)	FMB	Positive	Positive (SPM) Negative* (EPM)	Favorable Not favorable*
	SW-SO4	Negative	N/D, $\zeta_{r/w} \geq \zeta_{o/w}$ (SPM) Negative, $\zeta_{r/w} > \zeta_{o/w}$ (EPM)	N/D Favorable
	SWd40	Negative	N/D, $\zeta_{o/w} \geq \zeta_{r/w}$ (SPM) Negative, $\zeta_{r/w} > \zeta_{o/w}$ (EPM)	N/D Favorable
Inverse flooding (EST2)	SWd40	Negative	N/D, $\zeta_{o/w} \geq \zeta_{r/w}$ (SPM) Negative, $\zeta_{r/w} > \zeta_{o/w}$ (EPM)	N/D Favorable
	SW-SO4	Negative	N/D, $\zeta_{o/w} \geq \zeta_{r/w}$ (SPM) Negative, $\zeta_{r/w} > \zeta_{o/w}$ (EPM)	N/D Favorable
	FMB	Positive	Positive (SPM) Negative* (EPM)	Favorable Not favorable*

4.1.1. Zeta potential obtained by streaming potential measurements

In the studied COBR system, from streaming potential measurements (SPM), it is only possible to conclude without ambiguity that recovery is always favorable using FMB as both interfaces appear to be positive (Case 6 of Figure 3). For SW-SO4 and SWd40 brines, it is not possible to determine without ambiguity the polarity of the oil/water interface using SPM. Results indicate that oil/water zeta potential is either less negative than rock/water zeta potential or positive (mainly Case 2 of Figure 3).

The positive values for the oil/water zeta potential obtained in FMB are in good agreement with previous studies that have shown that positive oil/water interfaces may be more common than previously predicted in high salinity and temperature conditions [41,58], while the pH is higher than the typical isoelectric point of oils [59]. It is interesting to note that despite the same sign for both interfaces in FMB, the interpretation of k_r/Pc curves indicates that the rock appears to be intermediate-wet, which is in contradiction with the stabilization of a water film on the rock surface due to electrostatic repulsion between the two interfaces.

445 Two remarks can be done concerning this observation. Firstly, even if the sign of the macroscopic zeta
446 potential can be defined, it only provides a weighted average of the charge at the shear plane. This
447 value does not reflect the abundance of positive and negative surface sites in carbonates [42,60], and
448 many sites can still have an opposite polarity as the one of zeta potential. As a result, the conclusion
449 that electrostatic repulsion is expected due to the same polarity for rock/water and oil/water
450 interfaces may only be valid for some sites and is not generalizable to the entire rock. Hence,
451 depending on oil distribution on the different surface sites, the impact of electrostatic repulsion on
452 the stabilization of the water film and thus on oil recovery may be limited.

453 Secondly, even if electrostatic repulsion may occur at high salinity, the high ionic screening can result
454 in the formation of a very thin water film that could be unstable due to other attractive forces (Van
455 der Waals, Lewis acid-base forces, etc.). However, it has been shown that for high concentrations of
456 NaCl (> 1 M), the screening length of confined water film can be much larger than the one calculated
457 with the Debye–Hückel theory [61,62], which may complicate the interpretation of zeta potential in
458 terms of electrostatic forces through extended Derjaguin-Landau-Verwey-Overbeek (DLVO) theory
459 without considering solvation shell and steric effects.

460 Another point of discussion is the impact of the presence of oil on streaming potential. Figure 9
461 illustrates the water flow paths during streaming potential measurements at Sw = 1 and at Sor. Within
462 the porosity filled by water and oil presented in the form of films covering the pore walls, the water
463 flow paths are comparable between Sw = 1 and Sor. Hence, streaming potential value can directly be
464 impacted by oil polarity, as proposed by Jackson et al. [27], and the influence will depend on oil/water
465 surface polarity and the total rock surface covered by oil films within water flow paths.

466 However, we also suggest that oil can also indirectly contribute to streaming potential value by
467 inducing a change in rock exposed surface due to modification of water flow paths. Indeed, oil is not
468 homogeneously distributed within the porous media, especially for Estaillades rocks with macro- and

micro-porosity [44]. After waterflooding, oil can be trapped in some porosity with limited availability to water and, as a result, the water flow paths can partly differ between Sw = 1 and Sor.

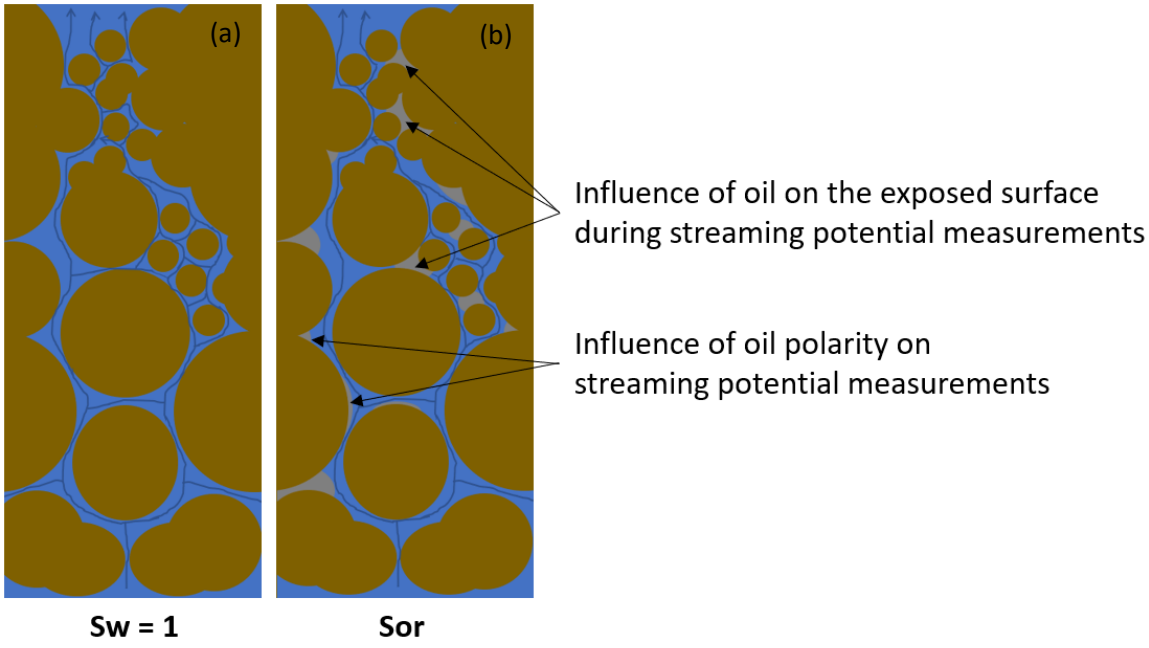

Figure 9. Schematic and simplified representation of COBR system with the water flow paths during streaming potential measurements (a) at Sw = 1 and (b) at Sor.

It appears then that the two measurements are not simply comparable as the total exposed surface ($A_{r/w}$ + $A_{o/w}$ from Eq. 9) is not similar. Depending on the heterogeneity of rock composition/crystallography, surface roughness, and the distribution of surface charges, the contribution of microscopic zeta potentials on the resulting macroscopic zeta potential can simply be different because of change in the exposed surface. Hence, the difference observed between Sw = 1 and Sor is not necessarily indicative of oil polarity but and can be also impacted by differences in rock surfaces exposed to water flow paths, which questions the validity of the hypothesis considered.

Finally, in any case, the hypothesis used to determine oil/water polarity from SPM does not provide a quantification of the magnitude of oil/water zeta potential as the rock surface fraction covered by water $A_{w/o}$ and the oil surface exposed to brine $A_{w/o}$ (Eq. 9) are difficult to determine. Hence, this complicates further interpretation. It is, for example, not possible to conclude if additional oil recovery is expected by increasing the magnitude of electrostatic repulsion forces when the recovery is already favorable with the first brine, as it is apparently the case for EST1. It is expected that increasing the

magnitude of repulsive forces will help in the stabilization of the water film, but this information cannot be obtained with SPM. As a result, it is not possible to conclude if the absence of additional oil recovery was expected in our conditions using streaming potential.

4.1.2. Zeta potential obtained by electrophoretic mobility measurements

As shown on

Table ***5***, based on EPM measurements, the recovery should not be favorable using FMB as rock/water interface is positive while oil/water interface appears negatively charged, whereas it should be favorable using either SW-SO4 or SWd40, as both rock/water and oil/water interfaces are negatively charged. Moreover, the results obtained from EPM clearly indicate more negative values for oil/water interfaces for SW-SO4 or SWd40 brines (Figure 8), which would correspond to Case 1 of Figure 3 and not to Case 2, as observed during SPM. Based on these results, the change in brine salinity should have resulted in additional oil recovery when switching to low salinity brines in tertiary mode (EST1, Figure 4a). However, we did not observe any significant recovery.

Many inconsistencies are then obtained when comparing the two methods. According to other studies, the oil/water interface generally exhibits a more negative value than the rock/water interface, especially in low salinity conditions [15,42,59,63,64], which is in agreement with our results using EPM. However, as these results were obtained by measuring the electrophoretic mobility of oil droplets in brine without the presence of rock, their applicability for core flooding experiments remains questionable.

Indeed, even for idealized porous media where the rock surface charge is homogeneously distributed and oil is present only as films on the rock surface, we can argue that the zeta potentials obtained by EPM may not always be representative of the oil/water interface observed during oil recovery. As illustrated in Figure 10, the presence of carbonate rock can influence the distribution of oil compounds, notably with the accumulation and adsorption of a fraction of surface-active agents, such

as asphaltenes, on rock surfaces during ageing [65]. Depending on their total content, the oil/water interface might partly be depleted in these compounds, which could explain the difference in magnitude of zeta potential values obtained between SPM and EPM.

This hypothesis may not be applicable in all conditions, especially when oil is in part refreshed during ageing process, but it can highlight the potential interest of the investigated hypothesis with SPM to determine oil/water polarity in more representative conditions. Recently, Collini and Jackson [66] have proposed a new method to determine the oil/water zeta potential using SPM in silanized Fontainebleau sandstone cores coated with crude oils, which could open the way for measurements in more representative conditions to obtain further insights on oil/water interface.

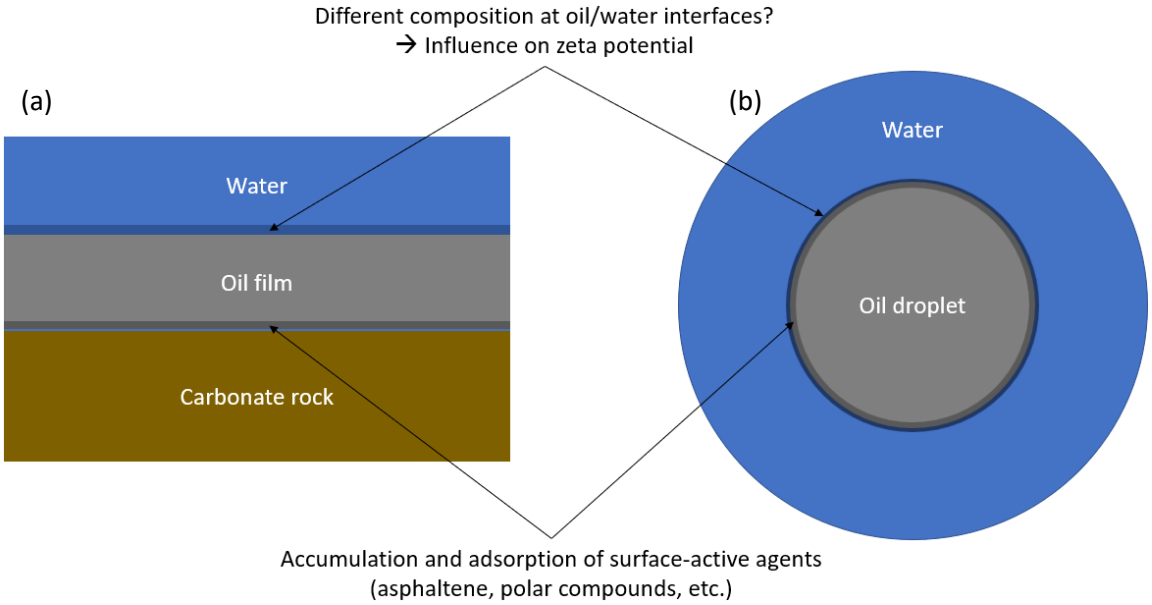

Figure 10. Schematic representation of measurements of oil/water interfaces with (a) streaming potential and (b) electrophoretic mobility. It illustrates the influence of carbonate rock on the distribution of oil surface-active agents, which can result in different compositions at oil/water interfaces depending on the method of measurement.

4.1.3. General conclusion on zeta potential

Irrespective of the chosen method to determine zeta potential, it is still unclear if it provides an accurate representation of the oil/water interface of interest during oil recovery. First, the stability of the interface is questionable as it may evolve during recovery, especially with the formation of water micro-droplets [21–24]. Hence, measurement of oil/water zeta potential may only represent a

snapshot of the interface, not representative of the entire recovery process. Secondly, the interface of interest for electrostatic considerations is the thin water film present between the rock surface and adsorbed oil, which is initially composed of connate water (here, FMB). During low salinity waterflooding, it is unknown if the initial film is easily replaced by the flooding solution or if it is only diluted by the transport of water through the oil phase due to osmotic gradient [67–69]. Hence, the composition of the film may significantly be different than the one of the flowing brines, and zeta potentials measured in low salinity brines may not be representative of this interface of interest.

Based on the different results obtained with SPM and EPM and the above discussion, it appears that zeta potential cannot be used as a unique indicator to predict the low salinity response.

4.2. Comparison with pore-scale network and importance of length and time scales

The same COBR system has been previously studied at pore-scale network using X-ray micro-computed tomography to obtain further insights on the mechanism of EOR by low salinity waterflooding, either in secondary mode [45] or in tertiary mode [46]. Using low-salinity brine in secondary mode, the evolution of oil recovery in the study of Selem et al. [45] is quite comparable to the one obtained in our study (Figure 4b). Especially, during the pressure bumps, the recovery is more important for the higher flowrates. This behavior was attributed to a redistribution of the fluid within the porous media: after having invaded the larger pores at initial flowrate, brine is progressively redirected to the smaller pores whereas oil is displaced into larger pores, which results in the increase in the total oil recovered [45].

Using low salinity brines in tertiary mode, Selem et al. have observed a 9 % increase in oil recovery after switching from high salinity to low salinity brine, but after the injection of several tens of PVs [46]. They evidenced the rapid formation of water micro-droplets in oil and the expansion of water films on the rock surface during injection of low salinity brine, so these phenomena are proposed to be the underlying mechanisms of wettability alteration [46]. However, the fluid occupancy maps'

555 change due to low salinity injection was different for pores and throats: the changes after low salinity
556 waterflooding were insignificant for the small throats while in small pores the oil was partially replaced
557 by water, which was attributed to wettability change. Hence, wettability alteration is not uniform
558 within the porosity and is more pronounced in the pore bodies than in the pore throats, which are
559 more critical for oil droplets propagations due to the higher capillary forces inside a restriction.

560 Also, it is unclear if the initial stabilization of the water film on rock surface is mainly related to
561 electrostatic repulsion rather than to the presence of water micro-dispersion. Indeed, the
562 spontaneous emulsification and growth of water-in-oil micro-droplets governed by osmotic effects
563 occur more rapidly as the salinity is decreased [21,70,71]. The presence of solid/liquid surface in the
564 vicinity of these structures can result in the formation of dewetting patterns on the solid surface, and
565 their possible coalescence can be responsible of the formation of a continuous water film [68]. As a
566 combination of the two mechanisms is still possible, it could be interesting to measure streaming
567 potential during experiments at pore scale network to determine if it can help in elucidating the
568 relative importance of electrostatic interactions and water micro-droplets on the initial formation of
569 the water film.

570 Nevertheless, irrespective of the underlying mechanism, this result is important as it clearly indicates
571 that EOR can be observed in this COBR system in tertiary mode, while we did not observe any
572 additional recovery at a bigger core scale (Figure 4). One reason for this difference can be related to
573 the different length and time scales under investigation [10]. Indeed, several tens of hours are
574 generally required to observe wettability alteration [72], which is typically the same order of
575 magnitude as the total duration of the injection of one brine at the initial flowrate in our experiments.
576 In addition, oil detachment from rock surface is not sufficient to observe additional oil recovery as oil
577 droplets must be transported through the porous media. Many phenomena such as oil coalescence,
578 trapping, remobilization, and banking must then be considered to eventually observe additional oil
579 recovery [10]. Increasing the size of the sample can drastically raise the importance of these

phenomena in EOR efficiency. However, they can't be captured only with zeta potential measurements.

The understanding of flow dynamics during wettability alteration in oil recovery experiments is still not fully understood. It was shown that wettability alteration can occur much earlier in flowing regions than in stagnant regions due to non-uniform mixing, leading to spatial variation of wettability conditions [73]. This spatial variation can notably be dependent on the capillary forces and the viscous dissipation in the interfaces [74] and on the pore morphology of the rock [75]. For Estaillades rock, it was shown that the medium heterogeneity creates stagnant zones with low-pressure values next to zones with high-pressure values, which results in considerable variation in the velocity distribution [76]. This could have largely affected the sweep efficiency and oil recovery in our experiments (Figure 4). More studies on the recirculation of the trapped phase are of prime interest [77], notably in the context of CSW. A better understanding of the flow dynamics will be helpful for improving oil recovery but also for interpreting the electrokinetic behavior.

Finally, we must note that the temporal aspect is crucial in laboratory scale experiments but not on field scale, as the operation generally lasts for months to years. The design of core flooding experiments has thus major influence on the results obtained during controlled salinity waterflooding. More studies are required to identify the most pertinent experimental design that can effectively result in EOR at pore scale while limiting false positive and false negative results. This could be an important step in the definition of standardized methods and protocols, which will be helpful for the intercomparison of results from different laboratories and, ultimately, a better understanding on the underlying mechanisms of CSW.

5. Conclusion

This study was devoted to investigating if zeta potential can be used as a unique indicator to predict the response of controlled salinity waterflooding in oil-water-carbonate systems.

The main conclusions are summarized as follow:

1. Oil recovery was more important when using formation brine in secondary mode compared to low salinity brine. Also, irrespective of the order of injection of the brines, almost no additional oil recovery was observed in tertiary mode.
2. Rock/water interface was negatively charged in low salinity conditions and positively charged in high salinity brine.
3. According to streaming potential measurements, oil/water interface appears positively charged in formation brine, suggesting that the recovery was already favorable using high-salinity brines. However, it was not possible to determine without ambiguity the polarity with low salinity brines and, consequently, to predict the impact on additional oil recovery.

   The interpretation of streaming potential measurements in terms of oil/water polarity was also questioned. We suggested that the change in zeta potential between fully water saturation and residual oil saturation is not necessarily dependent only on oil polarity as it can be also induced by a change in rock exposed surface and the distribution in water flow paths during measurements.
4. According to electrophoretic mobility measurements, the oil/water interface was negatively charged in low salinity brines, being even more negative than the rock/water interface. Hence, additional oil recovery should have been expected when switching to low salinity brines, whereas we did not observe any significant recovery.
5. The overall results suggest that zeta potential cannot be used as a unique indicator to predict the low salinity response of a COBR system.
6. A comparison with previous experiments at pore scale using the same COBR system confirmed the importance of length and time scales and of the flow dynamics in heterogeneous porous media on additional oil recovery.

   As long as the mechanism of the low-salinity effect is not well understood, we believe that the integration of streaming potential measurements in both core scale and pore network scale

experiments is of great interest to highlight the relative influence of electrostatic interactions on the overall mechanism of smart water injection methods.

CRediT author statement

Romain Rodrigues: Methodology, Software, Formal analysis, Investigation, Writing – Original Draft, Writing – Review & Editing, Visualization. **Michael Levant:** Conceptualization, Methodology, Software, Writing – Review & Editing, Supervision. **Alexandra Klimenko:** Conceptualization, Writing – Review & Editing, Supervision.

Declaration of Competing Interest

The authors declare that they have no known competing financial interests or personal relationships that could have appeared to influence the work reported in this paper.

Acknowledgments

The authors gratefully acknowledge TotalEnergies and more particularly Nicolas Agenet for funding and providing the material for this study. The authors thank Cyrille Hourcq, Patrice Fortané, Jean-Michel Gras, Michèle Joly and Géraldine Salabert for their help and advice for the installation of the experimental setup.

Abbreviations

CSW	Controlled salinity waterflooding
COBR	Crude oil-brine-rock
EOR	Enhanced oil recovery
EPM	Electrophoretic mobility measurements
EST	Estaillades
FMB	Formation brine
LSW	Low salinity waterflooding
OIP	Oil in place
PV	Pore volume
ROS	Remaining oil saturation
Sor	Residual oil saturation

SPM	Streaming potential measurements
Sw = 1	Fully water saturation
Swi	Irreducible water saturation
SW-SO4	Desulfated sea water
SWd40	40-times diluted sea water
SWIM	Smart water injection methods
WBT	Water breakthrough

646

A	Surface (m^2)
C	Coupling coefficient ($mV\ Pa^{-1}$)
C_i	Concentration in i ($mol\ L^{-1}$)
I	Ionic strength ($mol\ L^{-1}$)
k	Permeability (mD)
k_r	Relative permeability
L	Length (m)
n	Corey constant
Pc	Capillary pressure (bar)
Q	Flow rate ($m^3\ s^{-1}$)
r	Radius (m)
T	Temperature (K)
u_e	Electrophoretic mobility ($\mu m\ cm\ V^{-1}\ s^{-1}$)
ΔE	Potential difference / Streaming potential (mV)
ΔP	Pressure difference (Pa)
ε	Permittivity
ζ	Zeta potential (mV)
μ	Dynamic viscosity (Pa s)
σ	Conductivity ($S\ m^{-1}$)

Subscripts w, o and r states for water, oil and rock, respectively

647 Appendix A. Supplementary data

648 The following is the Supplementary data to this article:

649 References

650 [1] Ahmed T. Reservoir Engineering Handbook. Elsevier; 2018. https://doi.org/10.1016/C2016-0-
651 04718-6.

652 [2] Sheng JJ. Surfactant enhanced oil recovery in carbonate reservoirs. Enhanc. Oil Recover. F. Case
653 Stud., Gulf Professional Publishing; 2013, p. 281–99. https://doi.org/10.1016/B978-0-12-

386545-8.00012-9.

[3] Mogensen K, Masalmeh S. A review of EOR techniques for carbonate reservoirs in challenging geological settings. J Pet Sci Eng 2020;195:107889. https://doi.org/10.1016/J.PETROL.2020.107889.

[4] Xu Z-X, Li S-Y, Li B-F, Chen D-Q, Liu Z-Y, Li Z-M. A review of development methods and EOR technologies for carbonate reservoirs. Pet Sci 2020;17:990–1013. https://doi.org/10.1007/S12182-020-00467-5.

[5] Yousef AA, Al-Saleh S, Al-Kaabi A, Al-Jawfi M. Laboratory investigation of the impact of injection-water salinity and ionic content on oil recovery from carbonate reservoirs. SPE Reserv Eval Eng 2011;14.

[6] Yousef AA, Liu J, Blanchard G, Al-Saleh S, Al-Zahrani T, Al-Zahrani R, et al. Smartwater flooding: Industry's first field test in carbonate reservoirs. SPEREE J 2012;14:578–93.

[7] Katende A, Sagala F. A critical review of low salinity water flooding: Mechanism, laboratory and field application. J Mol Liq 2019. https://doi.org/10.1016/j.molliq.2019.01.037.

[8] Sohal MA, Thyne G, Søgaard EG. Review of recovery mechanisms of ionically modified waterflood in carbonate reservoirs. Energy and Fuels 2016;30:1904–14. https://doi.org/10.1021/acs.energyfuels.5b02749.

[9] Derkani M, Fletcher A, Abdallah W, Sauerer B, Anderson J, Zhang Z. Low salinity waterflooding in carbonate reservoirs: Review of interfacial mechanisms. Colloids and Interfaces 2018;2:20. https://doi.org/10.3390/colloids2020020.

[10] Bartels WB, Mahani H, Berg S, Hassanizadeh SM. Literature review of low salinity waterflooding from a length and time scale perspective. Fuel 2019;236:338–53. https://doi.org/10.1016/j.fuel.2018.09.018.

677 [11] Tetteh JT, Brady P V., Ghahfaorkhi RB. Review of low salinity waterflooding in carbonate rocks:
678 mechanisms, investigation techniques, and future directions. Adv Colloid Interface Sci
679 2020:102253. https://doi.org/10.1016/j.cis.2020.102253.

680 [12] Liu F, Wang M. Review of low salinity waterflooding mechanisms: Wettability alteration and its
681 impact on oil recovery. Fuel 2020;267:117112. https://doi.org/10.1016/j.fuel.2020.117112.

682 [13] Nande SB, Patwardhan SD. A review on low salinity waterflooding in carbonates: challenges
683 and future perspective. J Pet Explor Prod Technol 2021:1–19. https://doi.org/10.1007/S13202-
684 021-01361-5.

685 [14] Mohammed M, Babadagli T. Wettability alteration: A comprehensive review of
686 materials/methods and testing the selected ones on heavy-oil containing oil-wet systems. Adv
687 Colloid Interface Sci 2015;220:54–77. https://doi.org/10.1016/J.CIS.2015.02.006.

688 [15] Mahani H, Keya AL, Berg S, Bartels WB, Nasralla R, Rossen WR. Insights into the mechanism of
689 wettability alteration by low-salinity flooding (LSF) in carbonates. Energy and Fuels
690 2015;29:1352–67. https://doi.org/10.1021/ef5023847.

691 [16] Mahani H, Keya AL, Berg S, Nasralla R. Electrokinetics of carbonate/brine interface in low-
692 salinity waterflooding: Effect of brine salinity, composition, rock type, and pH on ζ-potential
693 and a surface-complexation model. SPE J 2017;22:53–68. https://doi.org/10.2118/181745-pa.

694 [17] Nasralla RA, Nasr-El-Din HA. Double-layer expansion: Is it a primary mechanism of improved oil
695 recovery by low-salinity waterflooding? SPE Reserv Eval Eng 2014.
696 https://doi.org/10.2118/154334-PA.

697 [18] Mahani H, Menezes R, Berg S, Fadili A, Nasralla R, Voskov D, et al. Insights into the impact of
698 temperature on the wettability alteration by low salinity in carbonate rocks. Energy and Fuels
699 2017;31:7839–53. https://doi.org/10.1021/acs.energyfuels.7b00776.

700 [19] Liu F, Wang M. Electrokinetic mechanisms and synergistic effect on ion-tuned wettability in oil-

brine-rock systems. Transp Porous Media 2021;140:7–26. https://doi.org/10.1007/S11242-021-01551-Z.

[20] Ding H, Rahman S. Experimental and theoretical study of wettability alteration during low salinity water flooding-an state of the art review. Colloids Surfaces A Physicochem Eng Asp 2017;520:622–39. https://doi.org/10.1016/J.COLSURFA.2017.02.006.

[21] Duboué J, Bourrel M, Carreras ES, Klimenko A, Agenet N, Passade-Boupat N, et al. Auto-emulsification of water at the crude oil/water interface: A mechanism driven by osmotic gradient. Energy and Fuels 2019;33:7020–7. https://doi.org/10.1021/acs.energyfuels.9b00946.

[22] Mehraban MF, Farzaneh SA, Sohrabi M, Sisson A. Fluid-fluid interactions inducing additional oil recovery during low salinity water injection in inefficacious presence of clay minerals. Fuel 2022;308:121922. https://doi.org/10.1016/J.FUEL.2021.121922.

[23] Mehraban MF, Farzaneh SA, Sohrabi M, Sisson A. Novel insights into the pore-scale mechanism of low salinity water injection and the improvements on oil recovery. Energy & Fuels 2020;34:12050–64. https://doi.org/10.1021/ACS.ENERGYFUELS.0C01599.

[24] Sohrabi M, Mahzari P, Farzaneh SA, Mills JR, Tsolis P, Ireland S. Novel insights into mechanisms of oil recovery by use of low-salinity-water injection. SPE J 2017;22:407–16. https://doi.org/10.2118/172778-PA.

[25] AlHammadi M, Mahzari P, Sohrabi M. Fundamental investigation of underlying mechanisms behind improved oil recovery by low salinity water injection in carbonate rocks. Fuel 2018;220:345–57. https://doi.org/10.1016/J.FUEL.2018.01.136.

[26] Bourrel M, Passade-Boupat N. Crude oil surface active species: Consequences for enhanced oil recovery and emulsion stability. Energy and Fuels 2018;32:2642–52. https://doi.org/10.1021/acs.energyfuels.7b02811.

[27] Jackson MD, Al-Mahrouqi D, Vinogradov J. Zeta potential in oil-water-carbonate systems and its impact on oil recovery during controlled salinity water-flooding. Sci Rep 2016;6:37363. https://doi.org/10.1038/srep37363.

[28] Revil A, Schwaeger H, Cathles LM, Manhardt PD. Streaming potential in porous media: 2. Theory and application to geothermal systems. J Geophys Res Solid Earth 1999;104:20033–48. https://doi.org/10.1029/1999jb900090.

[29] Jouniaux L, Ishido T. Electrokinetics in earth sciences: A tutorial. Int J Geophys 2012;2012. https://doi.org/10.1155/2012/286107.

[30] Navarro J, Raghuraman B, Bryant ID, Supp M. Streaming potential applications in oil fields. SPE Annu. Tech. Conf. Exhib., 2006, p. SPE-102106-MS. https://doi.org/10.2118/102106-MS.

[31] Cherubini A, Garcia B, Cerepi A, Revil A. Streaming potential coupling coefficient and transport properties of unsaturated carbonate rocks. Vadose Zo J 2018;17:180030. https://doi.org/10.2136/vzj2018.02.0030.

[32] Levant M, Agenet N, Santanach-Carreras E. Surface probing with streaming potential: The polymer flooding scenario. Transp Porous Media 2019;130:425–36. https://doi.org/10.1007/s11242-019-01318-7.

[33] Jackson MD, Vinogradov J. Impact of wettability on laboratory measurements of streaming potential in carbonates. Colloids Surfaces A Physicochem Eng Asp 2012;393:86–95. https://doi.org/10.1016/j.colsurfa.2011.11.005.

[34] Li S, Jackson MD, Agenet N. Role of the calcite-water interface in wettability alteration during low salinity waterflooding. Fuel 2020;276:118097. https://doi.org/10.1016/j.fuel.2020.118097.

[35] Al Mahrouqi D, Vinogradov J, Jackson MD. Zeta potential of artificial and natural calcite in aqueous solution. Adv Colloid Interface Sci 2017;240:60–76.

749 https://doi.org/10.1016/j.cis.2016.12.006.

750 [36] Song J, Wang Q, Shaik I, Puerto M, Bikkina P, Aichele C, et al. Effect of salinity, Mg2+ and SO42−
751 on “smart water”-induced carbonate wettability alteration in a model oil system. J Colloid
752 Interface Sci 2020;563:145–55. https://doi.org/10.1016/J.JCIS.2019.12.040.

753 [37] Alroudhan A, Vinogradov J, Jackson MD. Zeta potential of intact natural limestone: Impact of
754 potential-determining ions Ca, Mg and SO4. Colloids Surfaces A Physicochem Eng Asp
755 2016;493:83–98. https://doi.org/10.1016/j.colsurfa.2015.11.068.

756 [38] Rahbar M, Pahlavanzadeh H, Ayatollahi S, Manteghian M. Predicting the rock wettability
757 changes using solutions with different pH, through streaming potential measurement. J Pet Sci
758 Eng 2018;167:20–7. https://doi.org/10.1016/j.petrol.2018.03.080.

759 [39] Ricci M, Spijker P, Stellacci F, Molinari JF, Voïtchovsky K. Direct visualization of single ions in the
760 Stern layer of calcite. Langmuir 2013;29:2207–16. https://doi.org/10.1021/la3044736.

761 [40] Al Mahrouqi D, Vinogradov J, Jackson MD. Temperature dependence of the zeta potential in
762 intact natural carbonates. Geophys Res Lett 2016;43:11,578-11,587.
763 https://doi.org/10.1002/2016GL071151.

764 [41] Collini H, Li S, Jackson MD, Agenet N, Rashid B, Couves J. Zeta potential in intact carbonates at
765 reservoir conditions and its impact on oil recovery during controlled salinity waterflooding.
766 Fuel 2020;266:116927. https://doi.org/10.1016/j.fuel.2019.116927.

767 [42] Song J, Rezaee S, Guo W, Hernandez B, Puerto M, Vargas FM, et al. Evaluating physicochemical
768 properties of crude oil as indicators of low-salinity–induced wettability alteration in carbonate
769 minerals. Sci Rep 2020;10:3762. https://doi.org/10.1038/s41598-020-60106-2.

770 [43] Salimova R, Pourafshary P, Wang L. Data-driven analyses of low salinity waterflooding in
771 carbonates. Appl Sci 2021;11:6651. https://doi.org/10.3390/APP11146651.

772 [44] Gao Y, Qaseminejad Raeini A, Blunt MJ, Bijeljic B. Pore occupancy, relative permeability and
773 flow intermittency measurements using X-ray micro-tomography in a complex carbonate. Adv
774 Water Resour 2019;129:56–69. https://doi.org/10.1016/J.ADVWATRES.2019.04.007.

775 [45] Selem AM, Agenet N, Gao Y, Raeini AQ, Blunt MJ, Bijeljic B. Pore-scale imaging and analysis of
776 low salinity waterflooding in a heterogeneous carbonate rock at reservoir conditions. Sci Rep
777 2021;11:1–14. https://doi.org/10.1038/s41598-021-94103-w.

778 [46] Selem AM, Agenet N, Blunt MJ, Bijeljic B. Pore-scale imaging of tertiary low salinity
779 waterflooding in a heterogeneous carbonate rock at reservoir conditions. SPE Annu. Tech.
780 Conf. Exhib., Dubai, UAE: OnePetro; 2021, p. SPE-206357-MS.
781 https://doi.org/10.2118/206357-MS.

782 [47] Fievet P, Szymczyk A. Characterisation of electrical properties of membrane pore walls.
783 Comptes Rendus Chim 2002;5:493–505. https://doi.org/10.1016/S1631-0748(02)01413-3.

784 [48] Li S, Leroy P, Heberling F, Devau N, Jougnot D, Chiaberge C. Influence of surface conductivity
785 on the apparent zeta potential of calcite. J Colloid Interface Sci 2016;468:262–75.
786 https://doi.org/10.1016/j.jcis.2016.01.075.

787 [49] Bonto M, Eftekhari AA, Nick HM. Electrokinetic behavior of artificial and natural calcites: A
788 review of experimental measurements and surface complexation models. Adv Colloid Interface
789 Sci 2022:102600. https://doi.org/10.1016/J.CIS.2022.102600.

790 [50] Jouniaux L, Pozzi J-P. Permeability dependence of streaming potential in rocks for various fluid
791 conductivities. Geophys Res Lett 1995;22:485–8. https://doi.org/10.1029/94GL03307.

792 [51] Jougnot D, Roubinet D, Guarracino L, Maineult A. Modeling streaming potential in porous and
793 fractured media, description and benefits of the effective excess charge density approach. Adv.
794 Model. Interpret. Near Surf. Geophys., Springer, Cham; 2020, p. 61–96.
795 https://doi.org/10.1007/978-3-030-28909-6_4.

796 [52] Jougnot D, Mendieta A, Leroy P, Maineult A. Exploring the effect of the pore size distribution
797 on the streaming potential generation in saturated porous media, insight from pore network
798 simulations. J Geophys Res Solid Earth 2019;124:2018JB017240.
799 https://doi.org/10.1029/2018JB017240.

800 [53] Delgado A V., González-Caballero F, Hunter RJ, Koopal LK, Lyklema J. Measurement and
801 interpretation of electrokinetic phenomena. J Colloid Interface Sci 2007;309:194–224.
802 https://doi.org/10.1016/J.JCIS.2006.12.075.

803 [54] Austin J, Fernandes D, Ruszala MJA, Hill N, Corbett J. Routine, ensemble characterisation of
804 electrophoretic mobility in high and saturated ionic dispersions. Sci Rep 2020;10:1–12.
805 https://doi.org/10.1038/s41598-020-61624-9.

806 [55] Song J, Rezaee S, Zhang L, Zhang Z, Puerto M, Wani OB, et al. Characterizing the influence of
807 organic carboxylic acids and inorganic silica impurities on the surface charge of natural
808 carbonates using an extended surface complexation model. Energy & Fuels 2019;33:957–67.
809 https://doi.org/10.1021/ACS.ENERGYFUELS.8B03896.

810 [56] Hao X, Abu-Al-Saud M, Ayirala S, Elakneswaran Y. Influence of carbonate impurities on
811 smartwater effect: Evaluation of wettability alteration process by geochemical simulation. J
812 Mol Liq 2021;340:117165. https://doi.org/10.1016/J.MOLLIQ.2021.117165.

813 [57] Klimenko A, Molinier V, Bourrel M. Mechanisms underlying the adhesion of crude oil to mineral
814 surfaces: Relevance of oil-brine interactions. J Pet Sci Eng 2020;190:107036.
815 https://doi.org/10.1016/J.PETROL.2020.107036.

816 [58] Collini H, Jackson MD. Relationship between zeta potential and wettability in porous media:
817 Insights from a simple bundle of capillary tubes model. J Colloid Interface Sci 2022;608:605–
818 21. https://doi.org/10.1016/J.JCIS.2021.09.100.

819 [59] Bonto M, Eftekhari AA, Nick HM. An overview of the oil-brine interfacial behavior and a new

surface complexation model. Sci Rep 2019;9. https://doi.org/10.1038/s41598-019-42505-2.

[60] Heberling F, Bosbach D, Eckhardt JD, Fischer U, Glowacky J, Haist M, et al. Reactivity of the calcite-water-interface, from molecular scale processes to geochemical engineering. Appl Geochemistry 2014;45:158–90. https://doi.org/10.1016/j.apgeochem.2014.03.006.

[61] Smith AM, Lee AA, Perkin S. The electrostatic screening length in concentrated electrolytes increases with concentration. J Phys Chem Lett 2016;7:2157–63. https://doi.org/10.1021/ACS.JPCLETT.6B00867.

[62] Gaddam P, Ducker W. Electrostatic screening length in concentrated salt solutions. Langmuir 2019;35:5719–27. https://doi.org/10.1021/ACS.LANGMUIR.9B00375.

[63] Alotaibi MB, Yousef AA. The role of individual and combined ions in waterflooding carbonate reservoirs: Electrokinetic study. SPE Reserv Eval Eng 2017;20:077–86. https://doi.org/10.2118/177983-PA.

[64] Takeya M, Shimokawara M, Elakneswaran Y, Nawa T, Takahashi S. Predicting the electrokinetic properties of the crude oil/brine interface for enhanced oil recovery in low salinity water flooding. Fuel 2019;235:822–31. https://doi.org/10.1016/j.fuel.2018.08.079.

[65] Marcano MC, Kim S, Becker U. Surface interaction of crude oil, maltenes, and asphaltenes with calcite: An atomic force microscopy perspective of incipient wettability change. Appl Geochemistry 2020;113:104501. https://doi.org/10.1016/j.apgeochem.2019.104501.

[66] Collini H, Jackson M. Zeta potential of the crude oil-brine interface and implications for controlled salinity waterflooding. IOR 2021 - 21st Eur. Symp. Improv. Oil Recover., European Association of Geoscientists & Engineers; 2021, p. 1–12. https://doi.org/10.3997/2214-4609.202133090.

[67] Fredriksen SB, Rognmo AU, Fernø MA. Pore-scale mechanisms during low salinity waterflooding: Oil mobilization by diffusion and osmosis. J Pet Sci Eng 2018;163:650–60.

844 https://doi.org/10.1016/J.PETROL.2017.10.022.

845 [68] Bartels WB, Mahani H, Berg S, Menezes R, Van Der Hoeven JA, Fadili A. Oil configuration under
846 high-salinity and low-salinity conditions at pore scale: A parametric investigation by use of a
847 single-channel micromodel. SPE J 2017;22:1362–73. https://doi.org/10.2118/181386-pa.

848 [69] Crestel E. Déplacement de liquides par osmose étudié en microfluidique : application à la
849 récupération du pétrole. Université Paris Sciences et Lettres/ESPCI, PhD Thesis, 2019.

850 [70] Crestel E, Kvasničková A, Santanach-Carreras E, Bibette J, Bremond N. Motion of oil in water
851 induced by osmosis in a confined system. Phys Rev Fluids 2020;5:104003.
852 https://doi.org/10.1103/PHYSREVFLUIDS.5.104003.

853 [71] Duboué J, Bourrel M, Dusautoir T, Santanach Carreras E, Klimenko A, Agenet N, et al.
854 Fundamental investigation of auto-emulsification of water in crude oil: An interfacial
855 phenomenon and its pertinence for low salinity EOR. SPE Symp. Improv. Oil Recover.,
856 OnePetro; 2020, p. SPE-200357-MS. https://doi.org/10.2118/200357-MS.

857 [72] Mohammadi M, Nikbin-Fashkacheh H, Mahani H. Pore network-scale visualization of the effect
858 of brine composition on sweep efficiency and speed of oil recovery from carbonates using a
859 photolithography-based calcite microfluidic model. J Pet Sci Eng 2022;208:109641.
860 https://doi.org/10.1016/J.PETROL.2021.109641.

861 [73] Aziz R, Joekar-Niasar V, Martínez-Ferrer PJ, Godinez-Brizuela OE, Theodoropoulos C, Mahani H.
862 Novel insights into pore-scale dynamics of wettability alteration during low salinity
863 waterflooding. Sci Rep 2019;9:1–13. https://doi.org/10.1038/s41598-019-45434-2.

864 [74] Yang Y, Cai S, Yao J, Zhong J, Zhang K, Song W, et al. Pore-scale simulation of remaining oil
865 distribution in 3D porous media affected by wettability and capillarity based on volume of fluid
866 method. Int J Multiph Flow 2021;143:103746.
867 https://doi.org/10.1016/J.IJMULTIPHASEFLOW.2021.103746.

[75] Aziz R, Niasar V, Erfani H, Martínez-Ferrer PJ. Impact of pore morphology on two-phase flow dynamics under wettability alteration. Fuel 2020;268:117315. https://doi.org/10.1016/J.FUEL.2020.117315.

[76] El-Zehairy AA, Nezhad MM, Joekar-Niasar V, Guymer I, Kourra N, Williams MA. Pore-network modelling of non-Darcy flow through heterogeneous porous media. Adv Water Resour 2019;131:103378. https://doi.org/10.1016/J.ADVWATRES.2019.103378.

[77] Mohammadi Alamooti AH, Azizi Q, Davarzani H. Direct numerical simulation of trapped-phase recirculation at low capillary number. Adv Water Resour 2020;145:103717. https://doi.org/10.1016/J.ADVWATRES.2020.103717.